Front. Phys., 2014, 9(4): 439–445
DOI 10.1007/s11467-014-0433-1

RESEARCH ARTICLE

Study on quantitative analysis of slag based on spectral normalization of laser-induced plasma image

Zhi-Bo Ni[1], **Xing-Long Chen**[2], **Hong-Bo Fu**[1], **Jing-Ge Wang**[1], **Feng-Zhong Dong**[1,†]

[1] *Anhui Institute of Optics & Fine Mechanics, Chinese Academy of Sciences, Anhui Provincial Key Laboratory of Photonic Devices and Materials, Hefei 230031, China*

[2] *School of Instrument Science & Opto-Electronic Engineering, Hefei University of Technology, Hefei 230009, China*

Corresponding author. E-mail: †*fzdong@aiofm.ac.cn*

Received March 3, 2014; accepted May 4, 2014

To reduce the influence of laser-induced breakdown spectroscopy (LIBS) experimental parameter fluctuations to quantitative analysis of slag components, a normalization method using integral intensity of plasma image was proposed and a series of experiments with slag samples were performed. Mg II 279.55 nm, Ca II 396.85 and Ca I 422.67 nm were selected as analytical lines, and analytical curves of reference mass fractions versus spectral line intensities were established. With the increment of set threshold for edge extraction of plasma image, the determination coefficients and relative standard deviations of analytical curves were improved gradually and reached the optimum values when the threshold was equal to 10 000. Comparing with the results without normalization and normalized by whole spectrum area, the relativity between spectral line intensity and mass fraction can be enhanced efficiently after normalized by integral intensity of plasma image. The verification experiments with Ti alloy samples further confirmed the conclusions mentioned above.

Keywords laser-induced breakdown spectroscopy, analytical curve, plasma image, normalization

PACS numbers 42.62.Fi, 32.80.Lg

1 Introduction

Slag is an important production of smelting process and its components are very complicated [1]. The mass fractions of major components in slag are in the range of 30%–65% for CaO, 10%–40% for Al_2O_3 and 0.5%–13% for SiO_2. And slags from different smelting stages exhibit a significant heterogeneity in species distribution as well as varying color, cracks and ferrous oxide inclusions. Meanwhile, slag has several metallurgical functions, such as deoxidation, desulfurization and removal other impurities. Therefore, fast analysis of major components in slag plays decisive roles in assurance of smelting quality, improving recovery rate of steel and adjusting sequence of smelting operation. Nowadays, the widely used technique for analyzing slag components is XRF, which requires at least 20 minutes for sample preparation including sampling, delivering, crushing and pressing pellets. And a precise analysis takes additional time [2]. In order to improve the real-time of analysis results, laser-induced breakdown spectroscopy (LIBS), the appealing features of which include little to no sample preparation, in-situ and quick analysis and the capability to analyze any kind of sample, etc., is introduced [3–6].

However, the characteristics of laser-induced plasma can be affected by several factors, such as the fluctuation of laser energy, homogeneity of sample components, laser-sample interaction process and self-absorption, so the spectral line intensities of LIBS show obvious uncertainties. Even when experiments are performed with a homogeneous sample and under the same experimental conditions, the uncertainties are still obvious. This drawback has impeded the accuracy improvement of quantitative analysis and the further development of LIBS [7]. Thus, reducing the uncertainties has been one of the most important research topics. One common used method is averaging or accumulating of repeated measured spectra [8, 9]. However, because of nonlinear relationship between spectral line intensity and plasma characteristic parameters (plasma temperature, electron number density and particulate concentrations, etc.), linear averaging or accumulating of spectra may introduce some new errors. Another method is using plasma characteristic parameters to reduce the uncertainties. One of the outstanding representatives is the group of Zhe Wang

of Tsinghua University [10, 11]. After researching the relationship between spectral uncertainties and Characteristic parameters, they developed several algorithms to improve the stability of LIBS signal, and the effectiveness of their algorithms has been confirmed with brass alloy and coal, respectively. But their methods have not been used to improve the spectral stability of slag sample until now. Normalization is the third generally used method to minimize the uncertainties. One approach is normalizing the spectral line intensity with the peak intensity of an internal element [12, 13], and another approach is normalization with the whole spectrum area [14–16]. These methods can partially decrease the uncertainties induced by the experimental parameter fluctuations, but they also cannot overcome the effect of plasma free expansion. To explore new normalization approach for the improvement of spectral stability, Sturm *et al.* normalized the spectral line intensity by the diffraction intensity of the zeroth order which is detected by a PMT mounted at the zeroth order position of the spectrometer grating [17]. The determination coefficient of linear fitting for I/I(0th) versus reference mass fractions measured by XRF is greater than 0.97.

However, as for the commonly used grating spectrometer for LIBS, the grating is sealed in the instrument, and the zeroth order diffraction intensity cannot be detected by the ICCD. It is difficult for most researchers to obtain the zeroth order diffraction intensity. But the image of laser-induced plasma can be acquired easily, and the influence of experimental parameter fluctuations may be proportional to both spectral intensity and plasma image. In view of these facts, this study tries to demonstrate the relationship between spectral line intensity and plasma image using analytical curves. And results based on spectral line intensities normalized by integral intensities of corresponding plasma images are compared to those based on spectral line intensities without normalization and normalized by whole spectrum areas. Further verification experiments are also carried out with Titanium alloy.

2 Experimental setup

Assuming that plasma is optically thin and the local thermal equilibrium (LTE) is fulfilled during the temporal window of signal acquisition, the measured atomic or ionic characteristic spectral line intensity can be calculated by Boltzmann equation [18]:

$$I = F\frac{g_k \exp(-E_k/(k_{\mathrm{B}}T))}{U(T)}A_{ki}C_S \tag{1}$$

where F is the instrumental constant for fixed experimental conditions, and C_S is the total atomic or ionic number density. A_{ki} is transition probability, and the subscript k and i indicate the upper and lower energy level of characteristic line. g_k and E_k are the degeneracy and excitation energy of k level. $U(T)$ and k_{B} are partition function at temperature T and Boltzmann constant. For a specific spectral line and a given experimental condition, the ratio of identical spectral line intensity is

$$\frac{I_1}{I_2} = A\frac{C_{S1}U(T_2)}{C_{S2}U(T_1)}\exp\left(\frac{E_k}{k_{\mathrm{B}}T_2} - \frac{E_k}{k_{\mathrm{B}}T_1}\right) \tag{2}$$

which demonstrates the important roles of laser beam quality, ablation quantity, sample characteristics and collecting position in LIBS. Meanwhile, the size and spatial distribution of plasma may also be influenced by the factors mentioned above. To demonstrate the feasibility of correcting spectral line intensity with integral intensity of plasma image, a corresponding LIBS system shown in Fig. 1 is established. A 1064 nm Nd:YAG laser beam, the repetition rate and pulse width of which are 10 Hz and 8 ns respectively, is reflected by a mirror and focused by a convergent lens with focal length of 100 mm. The sample is placed on a x–y–z manually controlled stage. The distance between lens 1 and sample stage has been optimized by a series of experiments. The device to acquire spectra is mounted on one side of sample stage, and observes the plasma under an angle of about 20° to the sample surface. The emission spectrum is coupled into spectrometer of Andor ME5000, the spectral range of which is from about 230 to 975 nm with a wavelength accuracy of about 0.05 nm. An ICCD, the type of which is the same as that used in ME5000, is mounted on the other side to acquire plasma image under the angle of about 0° to sample surface. Delay time and gate width of both ICCDs are fixed at 1.5 μs and 1 μs, respectively. When plasma is generated by a single laser pulse, the corresponding emission signal and plasma image are acquired synchronously.

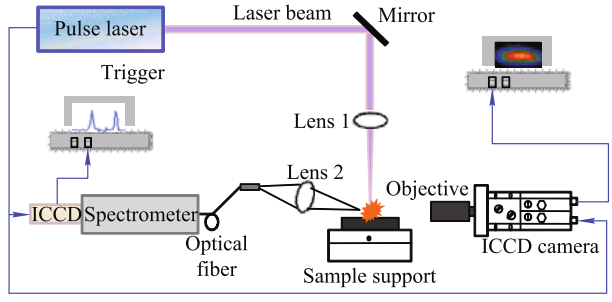

Fig. 1 Schematic setup of LIBS system.

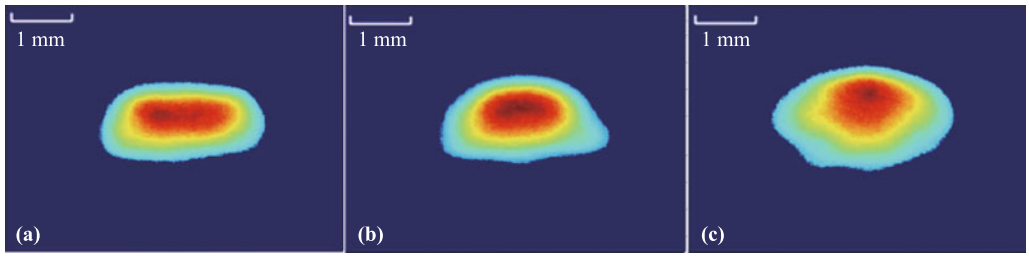

Fig. 2 Plasma images of different stage.

3 Results and discussion

3.1 Results of slag samples

The seven slag samples used in these series experiments are provided by Maanshan Iron & Steel Company Ltd. These samples are prepared after second molten and their appearances are similar to glass. The energy of Nd:YAG laser with maximum pulse energy of 500 mJ is fixed at 65 mJ in these experiments to avoid breaking up slag sample. The plasma images and spectra are synchronously acquired as a series, respectively. One series contains 50 group data, and each group data is corresponding to plasma induced by a single laser pulse. For each sample, four series data are acquired at different positions. Plasma images show that the variations of plasma in each series are almost the same, and three typical spatial distributions are illustrated in Fig. 2.

Plasmas induced by the earlier several pulses are very irregular and instable [Fig. 2(a)], and they become hemispherical with experiments gradually [Fig. 2(b)]. After about 40 pulses, longitudinal lengths of plasmas become larger and larger with the increment of ablation depth [Fig. 2(c)]. According to the typical generation and evolution process, the ideal shape of laser-induced plasma during early stage of expansion is close to hemisphere [19]. Then, the first selection criterion is that plasma shape must be close to hemisphere, and positions of spot centroids must be relatively stable. This criterion is to improve the consistency of relative collecting position for spectra. The second criterion is about the ratios of spectral line intensities belonging to different particles. For example, supposing that the statistical average ratio of Ca I 422.67 nm to Mg II 279.55 nm of 200 group signal is 6, but a ratio is 8 which deviates from 6 seriously, then the corresponding spectrum will be discarded. This criterion is to reduce the influence of inhomogeneity of components in samples.

A spectrum of slag sample taken from refinery cinder is shown in Fig. 3. For the spectrum induced by a single laser pulse, only a few spectral lines can be found, and independent spectral lines which do not have obvious self-absorption are even less. After careful selection, only spectral lines of Mg II 279.55 nm, Ca II 396.85 and Ca I 422.67 nm can meet our requirement, and the concentrations of MgO and CaO in 7 samples are shown in Table 1.

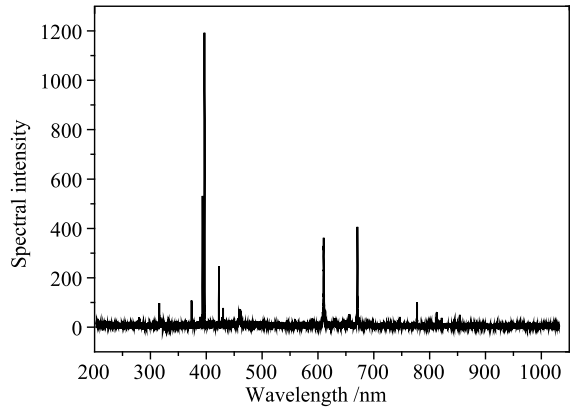

Fig. 3 Spectrum of refining slag sample induced by a single laser pulse.

Table 1 Concentrations of MgO and CaO in slag samples.

	Mass fractions /%						
MgO	2.36	2.37	7.73	5.38	4.87	5.70	5.78
CaO	37.09	44.65	40.03	48.93	47.50	62.56	63.46

In order to analyze the relativity between spectrum and plasma image, analytical curves basing on spectral line intensities normalized by integral intensities of corresponding plasma images are established and compared to analytical curves based on spectral line intensities without normalization and normalized by integral intensities of corresponding whole spectrum areas, respectively. The comparisons between different methods mentioned in this paper are based on the same set of data which are all selected by the two criterions mentioned above. To optimize the effect of normalization, series thresholds of ICCD background intensity are set to determine the edge of plasma image and distinguish it from background. Basing on these thresholds, we can calculate the integral intensities of plasma images. The variations of plasma images corresponding to thresholds varying from

2000 to 15 000 are shown in Fig. 4, in which 2000, 4000 and 6000, etc., are the thresholds. For a fixed threshold of 2000, there is a shadow under plasma, and the shadow becomes smaller and smaller with the increment of threshold and disappears when the threshold exceeds 8000. To find out the causes of shadow, the experiments are repeated using powder standard samples of the same slag. And in the later experiments we do not find the shadow. These results demonstrate that the shadow may be caused by shooting angle of ICCD and the characteristic of slag sample which is close to glass. With the increment of thresholds, the volume of plasma image decreases gradually.

After normalized by integral intensity of corresponding plasma image, the statistical average of spectral line intensities for each sample is obtained. The determination coefficients (R^2) of linear fitting for statistical average intensities versus mass fractions are illustrated in Fig. 5(a), and corresponding relative standard deviations (RSDs) are shown in Fig. 5(b), where squares, circles and triangles represent the results of Mg II 279.55 nm, Ca II 396.85 nm and Ca I 422.67 nm, respectively.

When the threshold of ICCD background intensity is set from 2000 to 10 000 step by step, R^2 and RSD which reflect the normalization effect improve gradually, and become worse when the threshold increase continuously. Take R^2 of spectral line Mg II 279.55 nm for example, it is smaller than 0.908 when the threshold is 2000. When the threshold is 10 000, the value exceeds 0.938, and it tends to stable with the further increment of threshold. For spectral line Ca I 422.67 nm, the threshold corresponding to optimum R^2 is 8000, which is smaller than that for Mg II 279.55 nm and Ca II 396.85 nm. The main reason may be the inhomogeneity of particles. Generally, ions assemble at central area of plasma where temperature is higher, but atoms assemble at area where temperature is a little lower [20, 21]. R^2 of analytical curves for Ca II 396.85 nm and Ca I 422.67 nm are smaller than that of Mg II 279.55 nm. The difference may be caused by self-absorption, because the mass fraction of CaO in samples is much greater than that of MgO. The RSDs of analytical curves for Mg II demonstrate the similar optimizing process as that of R^2, but their values are greater than those of Ca, which may be also relative to mass fractions.

For spectral line Mg II 279.55 nm, analytical curves based on spectral line intensities without normalization and normalized by integral intensities of corresponding plasma images are shown in Figs. 6(a) and (b), respectively. In these figures, circles represent relative spectral

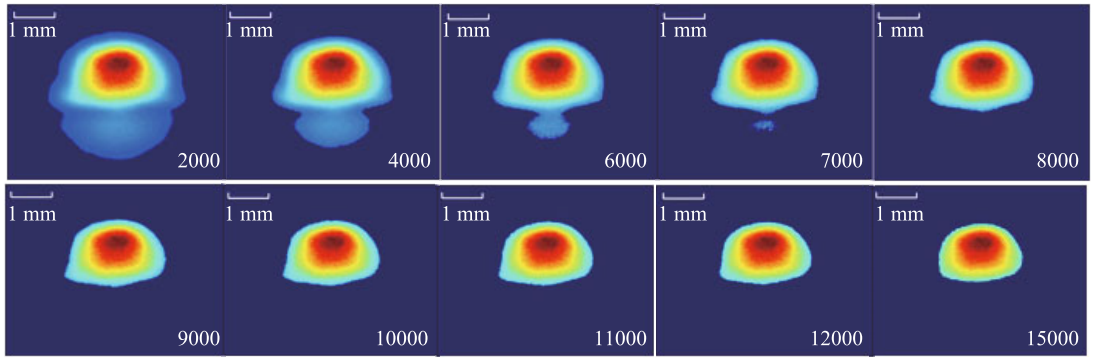

Fig. 4 Plasma image corresponding to different thresholds.

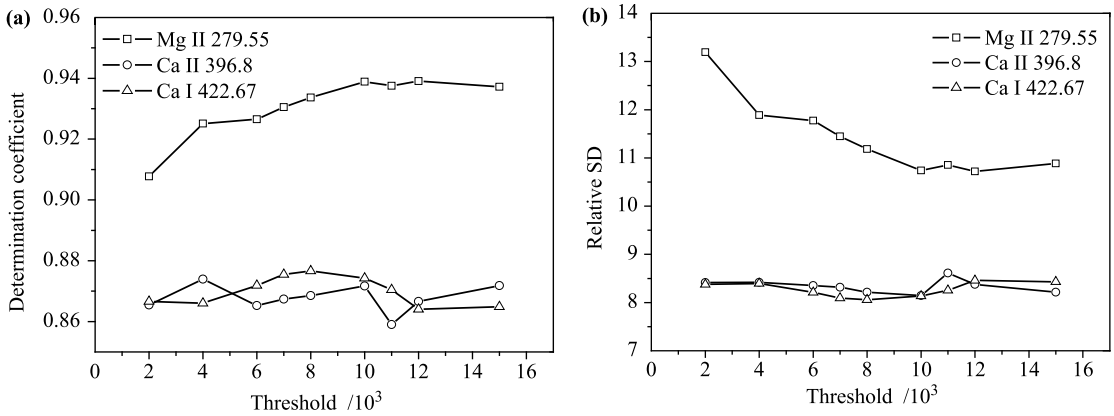

Fig. 5 Variations of linear fitting determination coefficients and relative standard deviations of analytical curves. **(a)** Variations of determination coefficients; **(b)** Variations of relative standard deviations.

line intensities of plasma induced by a single laser pulse, and triangles are corresponding to statistical average intensities. The R^2 of linear fitting for analytical curve of average intensities shown in Fig. 6(a) is 0.366, which indicates that there is not any obvious linear relationship. And the coefficient improves to 0.938 in Fig. 6(b), which demonstrates that the normalization can correct the spectral line intensity efficiently.

Analysis results of linear fitting for spectral line intensities of Ca I 422.67 nm versus mass fractions are shown in Fig. 7. In Fig. 7(a), circles represent the spectral line intensities induced by each single laser pulse after normalization with integral intensities of whole spectrum areas, and they are the intensities normalized by integral intensities of plasma images in Fig. 7(b). The meanings of triangles are the same as those shown in Fig. 6. In Fig. 7(a), the R^2 of linear fitting for statistical averages intensities is 0.400, and it improves to 0.939 in Fig. 7(b). The results shown in Figs. 6 and 7 demonstrate that, comparing to the other two methods mention above, normalization with integral intensity of corresponding plasma image can improve the relativity between spectral line intensity and mass fraction. The main reason may be that, the integral intensity of plasma image reflects the actual fluctuation of plasma radiation intensity. But the integral intensity of whole spectrum area is only a small part of the plasma radiation intensity, and can only reflect the signal fluctuation partially. Moreover, the influence of systematic noise fluctuation to integral intensity of whole spectrum area is more obvious, because the integral intensity of whole spectrum area is much lower than that of plasma image.

3.2 Verification results with Titanium alloy

In order to verify the effect of normalizing spectral line intensity with integral intensity of plasma image, a group of Titanium alloy standard samples provided by Central Iron & Steel Research Institute (CISRI) is tested. The acquisition mode during these experiments is the same with that used for signal acquisition of slag samples. For the spectra of Titanium alloy, there are lots of spectral lines belong to Ti II, but only one usable spectral line (Al I 396.15 nm) belonging to alloying elements can be found. The mass fractions of Titanium in 5 samples are relatively stable, so the verification experiment is based on spectral line Al I 396.15 nm. The mass fractions of Al and Ti are shown in Table 2.

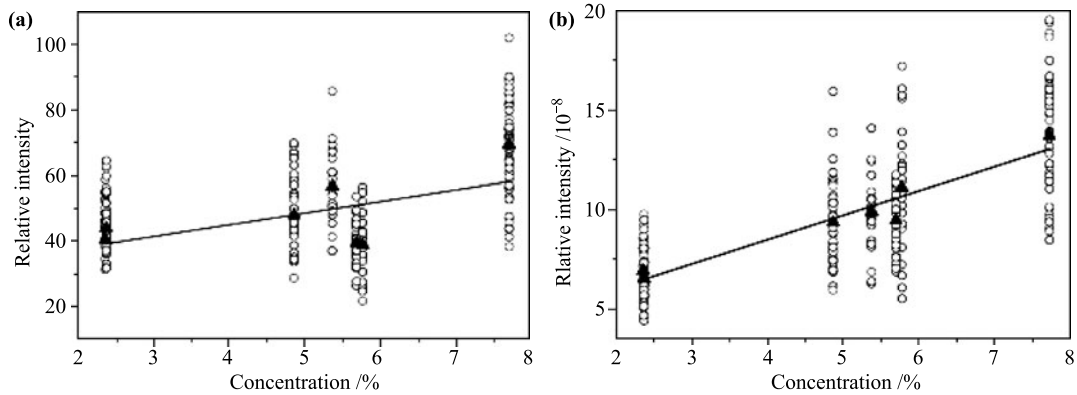

Fig. 6 Standard curves of Mg II 279.55 nm spectral line intensities versus reference mass fractions. **(a)** Without normalization; **(b)** Normalized by integral intensities of plasma images.

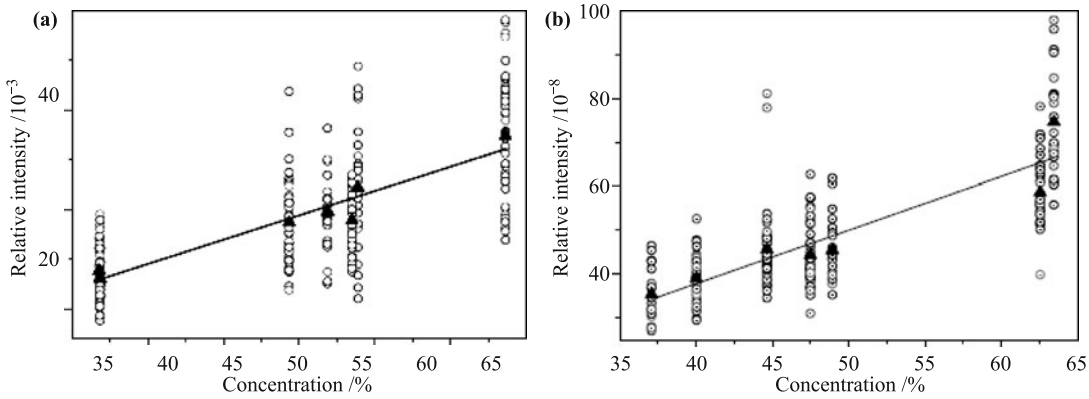

Fig. 7 Standard curves of Ca I 422.67 nm spectral intensities versus reference mass fractions. **(a)** Normalized by whole spectrum area; **(b)** Normalized by integral intensities of plasma images.

Table 2 Mass fractions of Al and Ti in Ti alloy.

Components	Mass fractions /%				
Al	4.59	5.59	6.25	7.05	7.64
Ti	87.87	88.14	88.04	88.77	88.52

When the thresholds of ICCD background intensity increase from 2000 to 10 000, variations of R^2 and RSDs are shown in Fig. 8. With the increment of thresholds, the normalization effect is optimized gradually. When the threshold is equal to 7000, the R^2 and RSD are optimal.

Analytical curves for Al_2O_3 are shown in Fig. 9. The R^2 of analytical curve without normalization is 0.899, and it improves to 0.953 when spectral line intensity is normalized by corresponding whole spectrum area. And the value reaches 0.987 when spectral line intensity is normalized by integral intensity of plasma image. It is apparent that normalization with integral intensity of plasma image can improve the relativity between spectral line intensity and mass fraction efficiently.

4 Conclusions

In the present work, spectra and plasma images of slag and Ti alloy samples are acquired, respectively. When spectral line intensity is normalized by integral intensity

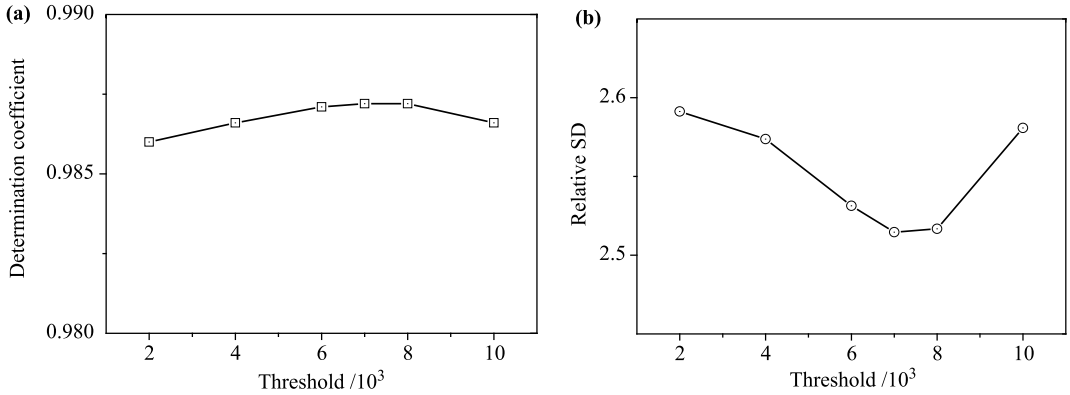

Fig. 8 Variations of R^2 and RSDs of linear fitting for analytical curves. **(a)** Variations of determination coefficients; **(b)** Variations of RSDs.

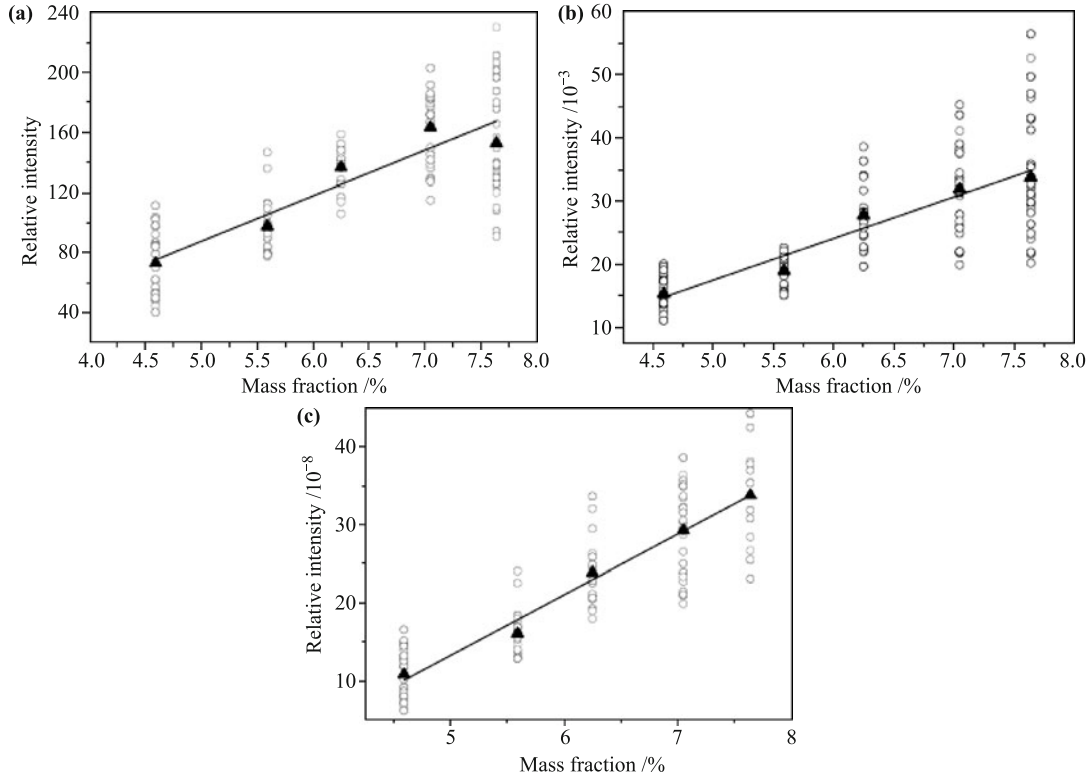

Fig. 9 Comparisons of analytical curves for Al. **(a)** Without normalization; **(b)** Normalized by whole spectrum area; **(c)** Normalized by integral intensity of plasma image.

of plasma image, the threshold of ICCD background intensity plays an important role. For a fixing threshold and the same set of spectral data after selection, analytical results of slag and Ti samples all indicate that, comparing to results without normalization and normalized by whole spectrum area, the determination coefficients and relative standard deviations can be optimized obviously when spectral line intensity is normalized by integral intensity of corresponding plasma image. These results demonstrate that, based on the selection criterions we have proposed, the influences of ablation quantity, sample characteristics and collecting position can be decreased deeply after normalization. Analysis results also indicate that, it is not always successful with the present normalization method especial for components of high mass factions. The main reason may be that the influence of self-absorption to spectral line intensities of major components is more obvious, and this needs further study in the future.

Acknowledgements We acknowledge the financial support from the National Natural Science Foundation of China (Grant No. 11075184) and the Knowledge Innovation Program of the Chinese Academy of Sciences (Grant No. Y03RC21124).

References

1. The Ministry of Human Resources and Social Security Office, Metallurgical Principle, Beijing: China Labour and Social Security Publishing House, 2011
2. M. Kraushaar, R. Noll, and H. U. Schmitz, Slag Analysis with Laser-Induced Breakdown Spectrometry, *Appl. Spectrosc.*, 2003, 57(10): 1282
3. R. Noll, Laser-Induced Breakdown Spectroscopy-Fundamentals and Applications, Springer, 2012
4. C. L. Moreno, S. Palanco, and J. J. Laserna, Quantitative analysis of samples at high temperature with remote laser-induced breakdown spectrometry using a room-temperature calibration plot, *Spectrochim. Acta B At. Spectrosc.*, 2005, 60(7–8): 1034
5. Z. Wang, T.B. Yuan, Z. Y. Hou, W. D. Zhou, J. D. Lu, H. B. Ding, and X. Y. Zeng, Laser-induced breakdown spectroscopy in China, *Front. Phys.*, 2014, DOI 10.1007/s11467-013-0410-0
6. F. Z. Dong, X. D. Chen, Q. Wang, L. X. Sun, H. B. Yu, Y. X. Liang, J. G. Wang, Z. B. Ni, Z. H. Du, Y. W. Ma, and J. D. Lu, Recent progress on the application of LIBS for metallurgical online analysis in China, *Front. Phys.*, 2012, 7(6): 679
7. S. C. Yao, J. D. Lu, C. L. Xie, P. Li, S. H. Pan, J. Li, and Y. Liu, Quantitative analysis of laser induced carbon plasma by intensity ratio calibration, *High Power Laser and Particle Beams*, 2008, 20(7): 1089 (in Chinese)
8. B. C. Windom and D. W. Hahn, Laser ablation-laser induced breakdown spectroscopy (LA-LIBS): A means for overcoming matrix effects leading to improved analyte response, *J. Anal. At. Spectrom.*, 2009, 24(12): 1665
9. L. C. Nunes, J. W. Batista Braga, L. C. Trevizan, P. Florencio de Souza, G. G. Arantes de Carvalho, D. S. Junior, R. J. Poppi, and F. J. Krug, Optimization and validation of a LIBS method for the determination of macro and micronutrients in sugar cane leaves, *J. Anal. At. Spectrom.*, 2010, 25(9): 1453
10. J. Feng, Z. Wang, L. Z. Li, Z. Li, and W. D. Ni, A PLS model based on dominant factor for coal analysis using laser-induced breakdown spectroscopy, *Anal. Bioanal. Chem.*, 2011, 400(10): 3261
11. Z. Wang, J. Feng, L. Li, W. Ni, and Z. Li, A multivariate model based on dominant factor for laser-induced breakdown spectroscopy measurements, *J. Anal. At. Spectrom.*, 2011, 26(11): 2289
12. B. Sallé, J. L. Lacour, P. Mauchien, P. Fichet, S. Maurice, and G. Manhes, Comparative study of different methodologies for quantitative rock analysis by Laser-Induced Breakdown Spectroscopy in a simulated Martian atmosphere, *Spectrochim. Acta B At. Spectrosc.*, 2006, 61(3): 301
13. F. Bredice, H. Sobral, M. Villagran-Muniz, H. O. Di Rocco, G. Cristoforetti, S. Legnaioli, V. Palleschi, A. Salvetti, and E. Tognoni, Real time measurement of the electron density of a laser generated plasma using a RC circuit, *Spectrochim. Acta B At. Spectrosc.*, 2007, 62(8): 836
14. L. Fornarini, F. Colao, R. Fantoni, V. Lazic, and V. Spizzicchino, Calibration analysis of bronze samples by nanosecond laser induced breakdown spectroscopy: A theoretical and experimental approach, *Spectrochim. Acta B At. Spectrosc.*, 2005, 60(7–8): 1186
15. F. J. Fortes, M. Cortes, M. D. Simon, L. M. Cabalin, and J. J. Laserna, Chronocultural sorting of archaeological bronze objects using laser-induced breakdown spectrometry, *Anal. Chim. Acta*, 2005, 554(1–2): 136
16. J. S. Huang and K. C. Lin, Laser-induced breakdown spectroscopy of liquid droplets: Correlation analysis with plasma-induced current versus continuum background, *J. Anal. At. Spectrom.*, 2005, 20(1): 53
17. V. Sturm, H. U. Schmitz, T. Reuter, T. Reuter, R. Fleige, and R. Noll, Fast vacuum slag analysis in a steel works by laser-induced breakdown spectroscopy, *Spectrochim. Acta B At. Spectrosc.*, 2008, 63(10): 1167
18. Z. Wang, L. Li, L. West, Z. Li, and W. Ni, A spectrum standardization approach for laser-induced breakdown spectroscopy measurements, *Spectrochim. Acta B At. Spectrosc.*, 2012, 68: 58
19. J. Yu, Q. L. Ma, V. Motto-Ros, W. Q. Lei, X. C. Wang, and X. S. Bai, Generation and expansion of laser-induced plasma as a spectroscopic emission source, *Front. Phys.*, 2012, 7(6): 649
20. W. Lei, Temporal and spatial characteristics of laser-induced plasma on organic materials and quantitative analysis of the contained inorganic elements, East China Normal University, Shanghai, 2012
21. W. Lei, V. Motto-Ros, M. Boueri, Q. Ma, D. Zhang, L. Zheng, H. Zeng, and J. Yu, Time-resolved characterization of laser-induced plasma from fresh potatoes, *Spectrochim. Acta B At. Spectrosc.*, 2009, 64(9): 891